ID-Blau: Image Deblurring by Implicit Diffusion-based reBLurring AUgmentation

Jia-Hao Wu[*,1]   Fu-Jen Tsai[*,2]   Yan-Tsung Peng[3]   Chung-Chi Tsai[4]   Chia-Wen Lin[2]   Yen-Yu Lin[1]

National Yang Ming Chiao Tung University[1]   National Tsing Hua University[2]

National Chengchi University[3]   Qualcomm Technologies, Inc.[4]

jiahao.11@nycu.edu.tw   fjtsi@gapp.nthu.edu.tw   ytpeng@cs.nccu.edu.tw

charles0184@gmail.com   cwlin@ee.nthu.edu.tw   lin@cs.nycu.edu.tw

Abstract

Image deblurring aims to remove undesired blurs from an image captured in a dynamic scene. Much research has been dedicated to improving deblurring performance through model architectural designs. However, there is little work on data augmentation for image deblurring. Since continuous motion causes blurred artifacts during image exposure, we aspire to develop a groundbreaking blur augmentation method to generate diverse blurred images by simulating motion trajectories in a continuous space. This paper proposes Implicit Diffusion-based reBLurring AUgmentation (ID-Blau), utilizing a sharp image paired with a controllable blur condition map to produce a corresponding blurred image. We parameterize the blur patterns of a blurred image with their orientations and magnitudes as a pixel-wise blur condition map to simulate motion trajectories and implicitly represent them in a continuous space. By sampling diverse blur conditions, ID-Blau can generate various blurred images unseen in the training set. Experimental results demonstrate that ID-Blau can produce realistic blurred images for training and thus significantly improve performance for state-of-the-art deblurring models. The source code is available at https://github.com/plusgood-steven/ID-Blau.

1. Introduction

Camera shake or object movements cause unpleasant motion blurs when we capture images. Such blurs are usually non-uniform, leading to locally and globally undesirable artifacts. Image deblurring aims to restore the sharpness of a blurred image, a highly ill-posed problem that has remained challenging over the past decades.

Image deblurring has reached remarkable progress with the rise of deep learning. Numerous methods based on con-
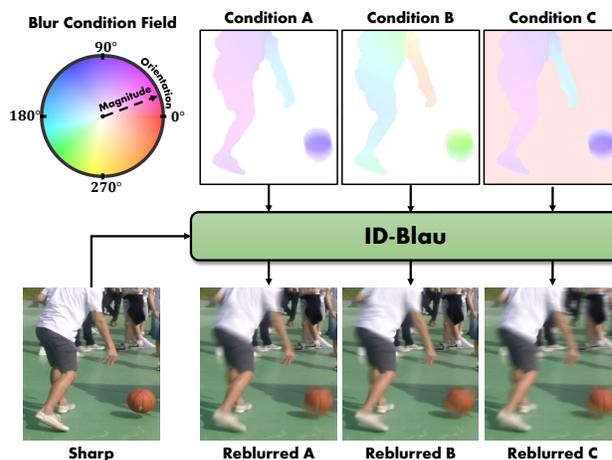

Figure 1. Examples of continuous reblurring by ID-Blau, where blur condition maps represent pixel-wise blur information, consisting of blur orientations and magnitudes, in a continuous space. ID-Blau can take a sharp image and a blur condition map to synthesize a blurred image, even unseen in the training set. Condition A is a blur condition map computed from the GoPro training set, which can be used to reblur a sharp image to generate a blurred image as provided in the training set. We can create Condition B and C based on A to synthesize new reblurred images, where Condition B is Condition A with rotated orientations, and Condition C is Condition A added with a camera motion blur.

volutional neural networks (CNNs) have rendered success in deblurring. These methods mostly adopted recurrent-based architectures, such as multi-scales [8, 18, 28], multi-patches [39, 41], and multi-temporal [20]. In addition to CNN-based methods, several studies have shown significant improvement using Transformers [3, 13, 31, 33, 40]. Transformers [32] utilize self-attention mechanisms to extract longer-range features than CNNs but require more memory. To overcome the high memory usage in the vanilla self-attention mechanism, some efficient attention mechanisms have been proposed, such as the channel-wise [40] and strip-wise attention [31] mechanisms.

___
* equal contribution

Although previous methods have improved deblurring performance through architectural designs, an effective data augmentation strategy for image deblurring has been less studied. A common strategy [42] is to synthesize blurred images through Generative Adversarial Networks (GANs) [10]. However, GANs usually generate uncontrollable results [14, 25, 37], constraining the potential of blur augmentation strategies. As a result, we resort to developing a stable and controllable blur augmentation method based on the inductive bias of motion blurs. Since continuous motions cause blur patterns during exposure, we attempt to implicitly characterize blurs, such as blur orientations and magnitudes, in a continuous space where we can sample blur trajectories to generate various blurred images. This enables us to generate various blurred images with specified blur conditions, devising a stable and controllable augmentation strategy for image deblurring.

In this paper, we propose **I**mplicit **D**iffusion-based re**BL**urring **AU**gmentation (**ID-Blau**) that can produce diverse blur and sharp training pairs for training to improve image deblurring performance. ID-Blau generates a realistic blurred image from a sharp image and a blur condition map to control the blur patterns through pixel-wise blur condition maps. Several examples are shown in Figure 1. To create blur condition maps, we implicitly represent blur information, including blur orientations and magnitudes, in a continuous space, where we can sample various blur conditions to simulate real blur trajectories during exposure. Compared to the GoPro training set [18], which accumulates consecutive sharp frames to generate explicit blurred images, our strategy can generate various blurred images with sampled blur conditions in the continuous blur condition field. In addition, motivated by the remarkable generation ability of diffusion models [12], ID-Blau adopts diffusion models to take implicit blur condition maps to generate realistic and controllable blurred images. Our experimental results demonstrate that ID-Blau, the proposed implicitly conditional diffusion model, can generate diverse blur and sharp training pairs for training, even for those unseen in the training set. As a result, it significantly improves the performance of existing deblurring models and performs favorably against state-of-the-art augmentation methods in this regard. Our contributions are summarized as follows:

- We propose ID-Blau, a stable and controllable blur augmentation strategy for enhancing dynamic scene image deblurring.

- We model a continuous blur condition field to implicitly represent blur orientations and magnitudes, where we can sample various pixel-wise blur condition maps to generate diverse reblurred images not provided in the training set.

- The proposed ID-Blau integrates pixel-wise blur condition maps into a diffusion model to generate high-quality reblurred images.

- Experimental results show that ID-Blau significantly improves existing deblurring models and performs favorably against state-of-the-art deblurring methods.

2. Related Work

2.1. Image Deblurring

The development of CNNs has advanced image deblurring remarkably. Several studies improved deblurring performance through recurrent networks, such as scale-recurrent [18, 28] and patch-recurrent [39, 41] networks. Specifically, Nah *et al*. [18] designed a scale-recurrent method to deal with image blur in a coarse-to-fine manner. Zhang *et al*. [41] developed a patch-recurrent method to leverage local information in a hierarchical deblurring network. Other than recurrent designs, Cho *et al*. [6] proposed an efficient deblurring model that rethinks the coarse-to-fine strategy in a single-forward model to reduce latency. Recently, motivated by the success of Vision Transformer (ViT) [7], several works [13, 31, 40] resorted to Transformer-based architectures to deblur an image. For example, Zamir *et al*. [40] utilized channel-wise attention to alleviate the tremendous memory load in the vanilla transformer for self-attention. Tsai *et al*. [31] proposed strip attention that exploits strip features to better extract blur features with various orientations and magnitudes. Kong *et al*. [13] proposed a frequency-based attention mechanism that utilizes element-wise multiplication in the frequency domain to replace the dot product in the spatial domain.

2.2. Deblurring through Reblurring

Besides focusing on architectural designs, some works [5, 15, 19, 42] enhanced deblurring performance through reblurring models. Chi *et al*. [5] and Liu *et al*. [15] utilized a reblurring network in meta-learning to achieve test-time adaptation. Nah *et al*. [19] proposed a reblurring network to amplify the blurs in a deblurred image while keeping sharp parts unchanged. It can be used to reinforce a deblurring network to generate a sharp result more accurately. Another potential strategy to improve deblurring models is to augment training pairs through reblurring models. Zhang *et al*. [42] exploited real-world blurry images to synthesize blurred images through GANs. However, GANs usually generate uncontrollable results, and GANs' unstable optimization process often increases the difficulty of training [2, 11, 17]. Besides, GANs' poor mode convergence [30, 35] makes them less effective in synthesizing diverse blurred images. In contrast, we propose to represent blur conditions in a continuous space implicitly and adopt

a diffusion method to generate diverse, realistic, and high-quality blurry images by considering arbitrarily enumerated blur conditions.

2.3. Diffusion Models

Diffusion models [12, 23, 26] have demonstrated their outstanding ability for image synthesis. Unlike GANs, diffusion models have a stable training strategy by synthesizing images through forward diffusion and backward denoising processes. The former gradually adds Gaussian noise to a clear image in multiple steps and generates noisy images in a sequence. The latter iteratively denoises the degraded images to restore the original image. Other than image synthesis, several studies have successfully applied diffusion models to low-level vision tasks, such as super-resolution [9, 24, 38], inpainting [1, 16, 36], and deblurring [4, 21, 34]. Specifically, Saharia *et al.* [24] conditioned the diffusion models on low-resolution images to reconstruct their high-resolution versions with visually pleasant quality. Whang *et al.* [34] conditioned the diffusion models on deterministic deblurring results to improve perceptual quality. Instead of constructing a restoration network based on diffusion models, we propose an implicitly conditional diffusion reblurring model to generate high-quality training data for improving deblurring performance for existing models. We can generate various blur conditions in a continuous space implicitly to control the proposed reblurring model to synthesize blurred images consistent with these conditions. By sampling the blur condition space, a set of diverse and high-quality blurred images can be generated to enrich the training set and enhance the performance of existing deblurring models.

3. Proposed Method

This section presents the proposed ID-Blau, which turns a sharp image into a blurred version based on a pixel-wise blur condition map. We characterize blurs with their orientations and magnitudes in a continuous space, where we can sample blur conditions for reblurring a sharp image. With the modeling, we can simulate blur trajectories yielded by continuous motion during exposure. It allows us to implicitly manipulate blur conditions to generate diverse blurred images unseen during training for data augmentation. In the data augmentation scenario, we can use ID-Blau to produce additional training data before optimizing deblurring models, so we do not need to run ID-Blau when optimizing deblurring models. The following details the computation of blur conditions and the training and sampling processes of ID-Blau for blurred image generation.

3.1. Blur Conditions

During exposure, continuous motion from a camera or scene objects may cause blur artifacts to captured images.
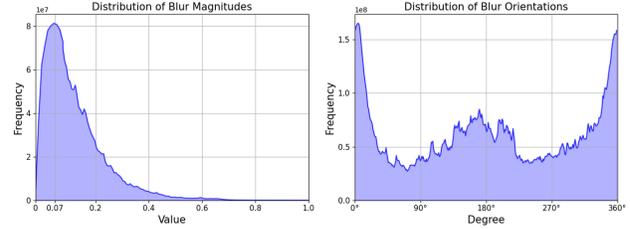

Figure 2. Illustration of distributions of blur magnitudes (left) and orientations (right) of the GoPro training set.

Thus, global and/or local blur trajectories can be found in such blurred images. To synthesize blurred images from their sharp counterparts, Nah *et al.* [18] proposed the GoPro dataset, approximating the continuous exposure through a blur accumulation function as

$$B = g(\frac{1}{T} \int_{t=1}^{T} V(t)dt) \simeq g(\frac{1}{N} \sum_{n=1}^{N} V[n]), \qquad (1)$$

where B, $V(t)$, T, N, and g denote the generated blurred frame, sharp frame at time t collected by a high-speed camera, exposure time, number of sampled sharp frames, and camera response function, respectively. The accumulation function aggregates a sharp image sequence $\mathbf{V} = \{V[1], ..., V[N]\}$ to generate one blurred image B. The center sharp frame $V[\frac{N+1}{2}]$ is assigned to the ground-truth image S for B, and N is typically an odd number.

Continuous motions of different objects may cause various blur patterns since they can move independently. We propose to characterize the blurs in an image into a blur condition map specifying a blur orientation and magnitude to each pixel. The blur condition map depicts a specific blur scenario for the blurred image by vectorizing blur for each pixel in a continuous field. By changing the blur condition map, we can simulate various blur scenarios and augment diverse blurred images to complement existing image deblurring datasets. To obtain the corresponding blur condition from a blurred image, we choose to average bidirectional optical flows from the sharp sequence $\mathbf{V}$ and then aggregate them by summation as

$$\mathcal{F} = \sum_{n=1}^{N-1} \frac{f_\theta(V[n], V[n+1]) - f_\theta(V[n+1], V[n])}{2},$$
(2)

where f_θ denotes the pre-trained optical flow estimation network [29], $\mathcal{F} = [u;v] \in \mathbb{R}^{H \times W \times 2}$ denotes the overall motion trajectories during exposure, where H and W are the image height and width, respectively. The tensor $\mathcal{F}$ records the horizontal and vertical motion trajectories in u and $v \in \mathbb{R}^{H \times W}$.

Next, we normalize $\mathcal{F}$ to obtain unit motion vectors and append one dimension of the magnitudes to make it a 3D tensor $C = [x;y;z] \in \mathbb{R}^{H \times W \times 3}$, where $x_{i,j} = \frac{u_{i,j}}{\sqrt{u_{i,j}^2 + v_{i,j}^2}}$
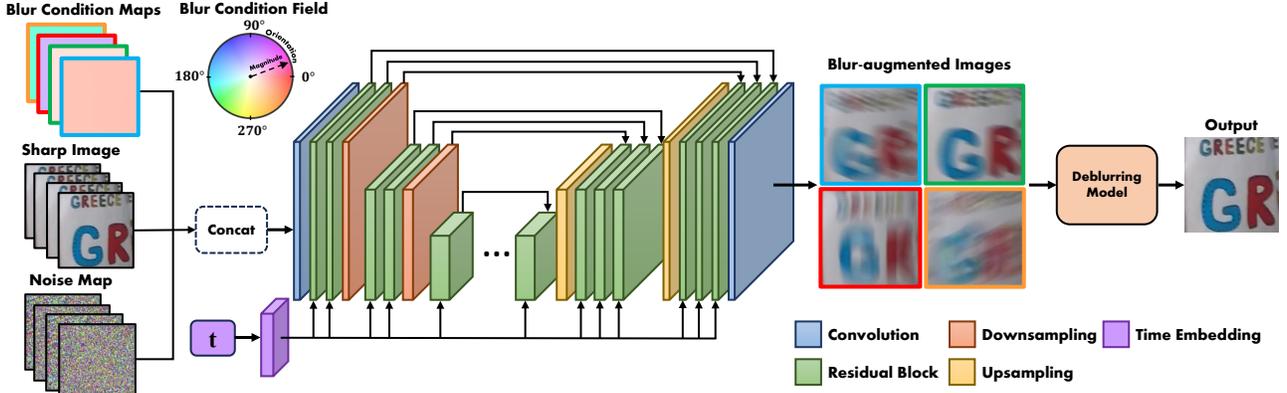
Figure 3. Reblurring process with ID-Blau. As the pie chart shows the blur condition field with orientations and magnitudes delineated in different colors, we visualize the process of generating blurred images with a set of blur condition maps. A sharp image paired with a blur condition map and a noise map is concatenated and fed into ID-Blau to produce a blurred image, where an MLP is used to encode the iteration index t as Time Embedding. Using ID-Blau can augment an image deblurring training set offline for optimizing a deblurring model and improving its performance.

and $y_{i,j} = \frac{v_{i,j}}{\sqrt{u_{i,j}^2+v_{i,j}^2}}$ respectively represent the horizontal and vertical blur orientations for a pixel (i,j), and $z_{i,j} = \frac{\sqrt{u_{i,j}^2+v_{i,j}^2}}{M}$ denotes its corresponding blur magnitudes. Here, M is set to the largest blur magnitude in a set of considered blur conditions to make $z \in [0,1]$.

Let C be the blur condition map for a blurred image B in a normalized continuous space, corresponding to its ground-truth image S. With the above modeling, we can construct a set of K blurred and sharp image pairs with their computed blur condition maps $\{B_n, S_n, C_n\}_{n=1}^K$ to train a reblurring model. It uses a sharp image S_n and a blur condition map C_n to produce the corresponding blurred image B_n, correlating the sharp image S_n and its blurred version B_n with our computed blur condition map C_n.

For example, we show the distribution of the blur magnitude and orientation of GoPro in Figure 2, indicating that the magnitude histogram peaks towards the left side, meaning most images are not heavily blurred. In contrast, the orientation has slight peaks around 0, 180, and 360 degrees, implying more blurs tend to be horizontal, but cases in other orientations can also be found. Training our reblurring model on such diverse data can correlate a blurred image with its computed blur information implicitly in a continuous blur condition field and empower the model to generate blurred images unseen in the original data by sampling different blur magnitudes and orientations. In the following, we describe optimizing the proposed diffusion-based reblurring model in ID-Blau.

3.2. ID-Blau

ID-Blau is developed based on a conditional diffusion model that takes a blur condition map C and a sharp image S as input to generate a blurred image B, as shown in Figure 3. Therefore, we can create various blur conditions

to augment data with realistic reblurred images unseen in the training set. To expedite the inference, we adopt the denoising diffusion implicit model (DDIM) [26], utilizing the same training procedure as DDPM [12] but accelerating the inference via a non-Markovian inference process.

Training Stage. Following DDPM [12], we perform a forward diffusion process and a backward denoising process to optimize ID-Blau. In the forward diffusion process, we gradually add Gaussian noise to a blurred image B over T iterations for generating a sequence of noisy images $\{B_1, ..., B_T\}$, where T is set to $2,000$. The sampling probability $q(B_{1:T}|B_0)$ is defined as

$$
\begin{aligned}
q(B_{1:T}|B_0) &= \prod_{t=1}^T q(B_t|B_{t-1}); \\
q(B_t|B_{t-1}) &= \mathcal{N}(B_t; \sqrt{\alpha_t}B_{t-1}, (1-\alpha_t)\mathrm{I}),
\end{aligned}
\tag{3}
$$

where $B_0 = B$ and $\{\alpha_t \in (0,1)\}$ is a set of hyperparameters that controls the noise variance over a sequence of steps. Instead of iteratively adding Gaussian noise to B, the forward diffusion process can be reparameterized as

$$
B_t = \sqrt{\overline{\alpha}_t}B_0 + (1-\sqrt{\overline{\alpha}_t})\epsilon,
\tag{4}
$$

where $\overline{\alpha}_t = \prod_{i=1}^t \alpha_i$ and $\epsilon \sim \mathcal{N}(0,\mathrm{I})$.

In the backward denoising process, the blurred image B is iteratively restored from the noisy image B_T through a denoising model ϵ_θ. When recreating a blurred image B from a noisy image, we condition the denoising model on its sharp counterpart S and the blur condition map C computed based on B. Thus, the denoising model learns to correlate a blurred image B and its sharp image S conditioned on the blur condition map C. The reverse conditional probability

| S | **ID-Blau**(S, C) | **ID-Blau**(S, C^1) | **ID-Blau**(S, C^2) | **ID-Blau**(S, C^3) | **ID-Blau**(S, C^4) |

Figure 4. Illustration of reblurred images with ID-Blau. It takes a sharp image S and a blur condition map $C = [x; y; z]$ as inputs to generate the corresponding blurred image. We show several generated blurred images by altering C, such as unit horizontal or vertical blur orientations, $C^1 = [1; 0; z]$ and $C^2 = [0; 1; z]$, horizontally inverse C as $C^3 = [-x; y; z]$, and $C^4 = [-x; y; 2z]$ with twice the magnitude for C^3.

is written as

$$p_\theta(B_{t-1}|B_t, S, C) = \mathcal{N}(B_{t-1}; \mu_\theta(B_t, S, C, t), \sigma_t^2 I);$$
$$\mu_\theta(B_t, S, C, t) = \frac{1}{\sqrt{\alpha_t}}(B_t - \frac{1 - \alpha_t}{\sqrt{1 - \overline{\alpha}_t}}\epsilon_\theta(B_t, S, C, t)),$$
$$(5)$$

where the Gaussian density function is parameterized with the mean of $\mu_\theta(B_t, S, C, t)$ and variance of $\sigma_t^2 = (1 - \alpha_t)$. To train the denoising model, we use the following objective function:

$$\mathcal{L} = \| \epsilon - \epsilon_\theta(\sqrt{\overline{\alpha}_t}B_0 + \sqrt{(1 - \overline{\alpha}_t)}\epsilon, S, C, t) \|_1, \quad (6)$$

where $\sqrt{\overline{\alpha}_t}B_0 + \sqrt{(1 - \overline{\alpha}_t)}\epsilon$ is the noisy image B_t at the t-th step. Figure 3 shows the architecture of the denoising model ϵ_θ.

Inference Stage. After optimizing the denoising model, ID-Blau can generate a blurred image B from a pure noisy image conforming to a Gaussian distribution $B_T \sim \mathcal{N}(0, I)$, a sharp image S, and a blur condition map C through the sampling procedure in DDIM. It can take any given blur condition map implicitly created to produce diverse blurred images unseen in the training set. The denoising process is given by:

$$B_{t-1} = \sqrt{\overline{\alpha}_{t-1}}(\frac{B_t - \sqrt{1 - \overline{\alpha}_t}\epsilon_\theta(B_t, S, C, t)}{\sqrt{\overline{\alpha}_t}})$$
$$+ \sqrt{1 - \overline{\alpha}_{t-1} - \sigma_t^2} \cdot \epsilon_\theta(B_t, S, C, t) + \sigma_t z,$$
$$(7)$$

where $\sigma_t = 0$, making the process deterministic. Through DDIM, we set the number of iterations during sampling to 20 without excessively sacrificing the image generation quality.

Figure 4 shows examples of generating different blurred images from a sharp image S by ID-Blau. That is, given a blur condition map $C = [x; y; z]$ and a sharp image S,

ID-Blau can produce a blurred image $B = $ **ID-Blau**(S, C). Additionally, we create four blur condition maps based on C for further demonstration, including unit horizontal or vertical blur orientations, $C^1 = [1; 0; z]$ and $C^2 = [0; 1; z]$, horizontally inverse C as $C^3 = [-x; y; z]$, and $C^4 = [-x; y; 2z]$ with twice the magnitude for C^3.

Besides, we have more examples to demonstrate the generalizability of ID-Blau by utilizing sharp images not in the training set to yield different blurred images in the supplementary material. These visuals attest that ID-Blau can effectively generate controllable and realistic blurred images. Thus, it can augment training data to improve image deblurring performance.

4. Experiments

4.1. Implementation Details

ID-Blau. We adopt the GoPro training set [18], which contains 2,103 blurred and sharp images for training ID-Blau. The training also requires the blur condition maps computed based on the blurred images. We use a batch size of 32 and randomly crop images with the size of 128×128 for training 5,000 epochs. We adopt the Adam optimizer and maintain a fixed learning rate of $1e^{-4}$. After optimizing ID-Blau, we utilize sharp images in the GoPro training set and create extra blur condition maps to produce additional 10,000 1280×720 blurred images by randomly modifying blur orientations and magnitudes based on the originally computed blur condition maps. The newly generated 10,000 blurred and sharp pairs can largely enrich the GoPro training set to enhance the performance of a deblurring model. ID-Blau has 9.5 million parameters, and it takes 3.4 seconds to generate a 1280×720 blurred image on an Nvidia 3090 graphics card.

The authors from the universities in Taiwan completed the experiments on the datasets.

Table 1. Evaluation results on the GoPro, HIDE, and RealBlur datasets, where "Baseline" and "+ID-Blau" denote the deblurring performances without and with ID-Blau, respectively.

Model		GoPro		HIDE		RealBlur-J		RealBlur-R		Average Gain	
		PSNR	SSIM	PSNR	SSIM	PSNR	SSIM	PSNR	SSIM	PSNR	SSIM
MIMO-UNet+	Baseline	32.44	0.957	30.00	0.930	31.92	0.919	39.10	0.969		
	+ID-Blau	**32.93 (+0.49)**	**0.961**	**30.68 (+0.68)**	**0.938**	**31.96 (+0.04)**	**0.921**	**39.38 (+0.28)**	**0.971**	**+0.37**	**+0.004**
Restormer	Baseline	32.92	0.961	31.22	0.942	32.88	0.933	40.15	**0.974**		
	+ID-Blau	**33.51 (+0.59)**	**0.965**	**31.66 (+0.44)**	**0.947**	**33.11 (+0.23)**	**0.937**	**40.31 (+0.16)**	0.974	**+0.36**	**+0.003**
Stripformer	Baseline	33.08	0.962	31.03	0.940	32.48	0.929	39.84	0.974		
	+ID-Blau	**33.66 (+0.58)**	**0.966**	**31.50 (+0.47)**	**0.944**	**33.77 (+1.29)**	**0.940**	**41.06 (+1.22)**	**0.977**	**+0.89**	**+0.006**
FFTformer	Baseline	34.21	0.969	31.62	0.946	32.62	0.933	40.11	0.973		
	+ID-Blau	**34.36 (+0.15)**	**0.970**	**31.94 (+0.32)**	**0.949**	**32.88 (+0.26)**	**0.934**	**40.45 (+0.34)**	**0.975**	**+0.27**	**+0.002**
Average Gain		**+0.45**	**+0.003**	**+0.48**	**+0.005**	**+0.46**	**+0.005**	**+0.50**	**+0.002**	-	-

Deblurring models. We adopt four prominent deblurring models, including MIMO-UNet+ [6], Restormer [40], Stripformer [31], and the state-of-the-art FFTformer [13] to demonstrate the effectiveness of ID-Blau. Following previous works, we evaluate deblurring performance on the GoPro, HIDE [27], and RealBlur [22] datasets. The GoPro dataset comprises $2,103$ training pairs and $1,111$ testing pairs. The HIDE dataset contains $2,025$ image pairs only for testing. The RealBlur dataset contains $3,758$ training pairs and 980 testing pairs. We pre-train each deblurring model on the generated $10,000$ training pairs for 500 epochs. After that, we fine-tune each deblurring model on the GoPro training set following its default training setting and then evaluate it on the GoPro testing set and the HIDE dataset. Besides, we fine-tune each deblurring model on the RealBlur training set to demonstrate the effectiveness of ID-Blau on real-world blurred images. Since all compared methods utilized the GoPro and RealBlur training sets for evaluating the RealBlur testing set, ID-Blau ensures a fair comparison without relying on extra training data.

4.2. Experimental Results

Quantitative Results. We compare the deblurring performance of four baselines and their ID-Blau-powered versions in Table 1, where "Baseline" and "+ID-Blau" denote the deblurring performance without and with ID-Blau, respectively. Table 1 shows that ID-Blau significantly improves four prominent deblurring models, including MIMO-UNet+ [6], Restormer [40], Stripformer [31], and the state-of-the-art FFTformer [13], on the GoPro, HIDE, and RealBlur datasets. ID-Blau enhances those models' performance in PSNR by 0.45dB, 0.48dB, 0.46dB, and 0.50dB averagely on GoPro, HIDE, RealBlur-J, and RealBlur-R, respectively. In particular, with ID-Blau, the state-of-the-art performance has been advanced to 34.36dB ($+0.15$dB) on GoPro, 31.94dB ($+0.32$dB) on HIDE, 33.77dB ($+0.89$dB) on RealBlur-J, and 41.06dB ($+0.72$dB) on RealBlur-R, where the enhanced FFTformer achieves new SOTA results on GoPro and HIDE, and

the enhanced Stripformer performs the best on ReaBlur-J and RealBlur-R. These comprehensive quantitative results demonstrate that ID-Blau significantly improves the performances of the four deblurring models on four widely-used datasets, showcasing ID-Blau's effectiveness and robustness as a data augmentation scheme for deblurring.

Qualitative Results. Figure 5 compares the visual qualities of the results with the four deblurring baselines (denoted by "Baseline") and their ID-Blau-powered versions (denoted by "+ID-Blau") on GoPro and HIDE. The results show that ID-Blau significantly enhances deblurring visual qualities compared to the Baselines. Besides, we demonstrate visuals of deblurring models on RealBlur-J in Figure 6. We also demonstrate deblurring results on real-world blurry images [42] in the supplementary material.

4.3. Ablation Studies

We analyze the impact of ID-Blau on deblurring performance using GoPro. For efficiency, we train MIMO-UNet [6], a compact version of MIMO-UNet+, for $1,000$ epochs for analysis. If not specifically mentioned, "Baseline" denotes MIMO-UNet trained on the GoPro training set without using any additional augmented data samples.

Effect of Augmenting Blur Orientations. Table 2 shows the effect of augmenting blur orientations with different angles on deblurring performance. To this end, with the original blur magnitudes, we rotate the blur orientations $[x; y]$ by four fixed angles ($30°$, $60°$, $90°$, and $120°$) plus a randomly selected angle for each produced blurred image (denoted "Random"). The results indicate that blur augmentation with all specific/random angles achieves performance improvements similar to those of Baseline. This suggests no need to employ specific angles in blur condition maps for augmentation. For implementation convenience, we randomly alter blur orientations $[x; y]$ to $[-x; y]$, $[x; -y]$, or $[-x; -y]$ to augment blurred images with different orientations, achieving a similar performance improvement as well.

Figure 5. Qualitative results on the GoPro testing set (left) and the HIDE dataset (right).
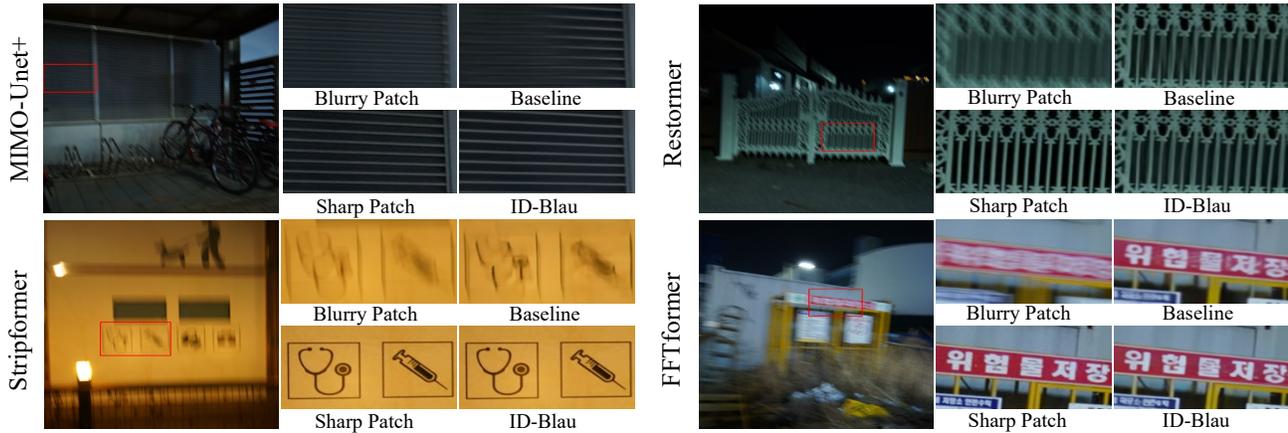

Figure 6. Qualitative results on the RealBlur-J testing set.

Table 2. Impact of modifying blur orientations on deblurring performance in PSNR (dB).

	Baseline	30°	60°	90°	120°	Random
PSNR	31.22	31.99	32.00	31.97	31.95	31.96

Effect of Adjusting Blur Magnitudes. Figure 7 illustrates the effect of modifying blur magnitudes on the deblurring performance. We first investigate the distribution of blur magnitudes within GoPro, in which most blurred images have blur magnitudes around with the peak at 0.07. Subsequently, we augment blurred images with different blur magnitudes by shifting the peak of magnitude distribution to different values, including 0.07, 0.15, 0.2, 0.3, and 0.4. The results demonstrate that shifting the distribution's peak to a larger value causes decreased performance, indicating that generating blurred images that deviate from the original distribution of the dataset leads to a performance drop. Therefore, we modify blur magnitudes but keep the peak of blur magnitudes at around 0.07.

Effect of the Number of Augmented Samples. The left plot of Figure 8 shows the impact of the number of augmented training pairs by ID-Blau on the deblurring performance. The performance gain of ID-Blau over that of the baseline, trained on GoPro without augmentation, increases from 0.53dB to 0.87dB with the number of augmented data samples (from 2, 500 to 20, 000), demonstrating ID-Blau's ability to improve the deblurring performance without the need of collecting additional training data samples. Augmenting 10, 000 additional samples (476% of the original data size) achieves a reasonable tradeoff between the performance gain and training complexity. Since ID-Blau does not require extra training samples but consumes additional training complexity, we also investigate whether the performance improvements come from the additional training complexity. As shown in the right plot of Figure 8, ID-Blau stably outperforms the baseline with the same training complexities (*i.e.*, the numbers of training iterations), where both the pre-training and fine-tuning process of ID-Blau are considered. Both the above experiments verify the performance gain with ID-Blau-based augmentation.

Effect of the Continuous Reblurring by ID-Blau. Figure 9 shows two blurred images from GoPro and their reblurred versions by ID-Blau. Since GoPro's blurred images are generated by blur accumulation as in (1), they contain unnaturally overlapping artifacts. In contrast, ID-Blau can generate similar blurred images by simulating continuous motion trajectories, yielding more realistic blurred images without such discontinuous overlapping artifacts. There-
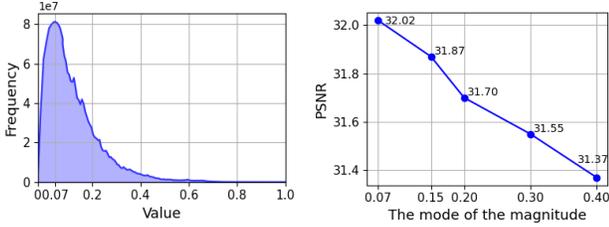
Figure 7. Left: Distribution of blur magnitudes within the GoPro training set. Right: Illustration of the effect of altering the distribution's mode at different values on the deblurring performance.
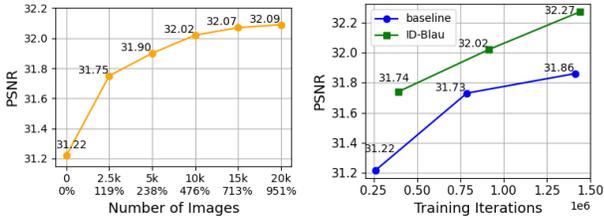

Figure 8. Deblurring performance (PSNR) versus the number of augmented samples by ID-Blau (left) and versus the number of training iterations (right).
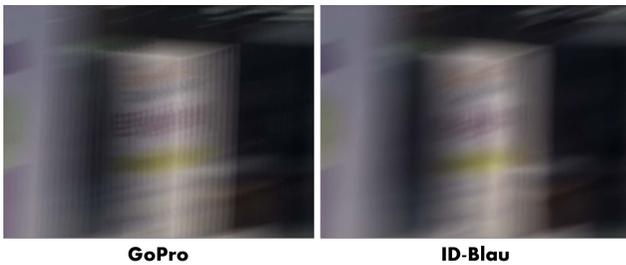

Figure 9. Left: Blurry image in GoPro dataset. Right: Blurry image generated by ID-Blau. ID-Blau can generate blurry images without overlapped artifacts compared to the GoPro dataset.

fore, ID-Blau can generate more realistic blurred images to improve the deblurring models' performances.

Performance Gain with a Diffusion Process. In ID-Blau, we adopt the diffusion process in [12] to generate blurred versions of sharp images with specified blur conditions. However, without the diffusion process, we can still utilize the same reblurring model to learn the mapping from a sharp image plus a computed blur condition map to the corresponding blurred image with the typical L1 loss function. To analyze the impact of ID-Blau with or without the diffusion process on deblurring performance, in Table 3, we compare Baseline (the same as in Figure 8), "w/ ID-Blau†," (ID-Blau without diffusion), and "w/ ID-Blau" (our model). The results show that "w/ ID-Blau†" and "w/ ID-Blau" improve the Baseline by 0.57dB and 0.80dB, respectively, and the diffusion model achieves 0.23dB additional performance gain.

Comparison between ID-Blau- and BGAN-based Augmentation. Besides, we compare the performance gains of ID-Blau and that of BGAN [42], a representative re-

Table 3. Effectiveness of using a diffusion model in ID-Blau on MIMO-UNet's performance in PSNR (dB), where "ID-Blau†" denotes the proposed ID-Blau without its diffusion process.

Model	Baseline	w/ ID-Blau†	w/ ID-Blau
PSNR	31.22	31.79	32.02

Table 4. Comparison between ID-Blau and BGAN regarding the DBGAN's performance in PSNR (dB), where ID-Blau† denotes the proposed ID-Blau without its diffusion process.

Model	Baseline	w/ BGAN	w/ ID-Blau†	w/ ID-Blau
PSNR	30.43	30.92	31.57	**31.67**

blurring GAN for augmenting blurred images to improve the DBGAN deblurring model. To fairly compare ID-Blau with BGAN, we utilize ID-Blau to improve DBGAN's deblurring performance. In Table 4, "Baseline" denotes DBGAN's performance trained on GoPro, and "w/ BGAN" denotes DBGAN's performance with BGAN-augmented data. "w/ ID-Blau†" and "w/ ID-Blau" denote DBGAN's performance using ID-Blau-augmented data without and with the diffusion process, respectively. Note that GAN-based methods tend to generate unpredictable and uncontrollable blurred images, whereas ID-Blau can generate controllable results based on specified blur conditions. As a result, "w/ ID-Blau†" and "w/ ID-Blau" improve the PSNR performance of DBGAN by 1.14dB and 1.24dB. Thanks to the proposed continuous blur condition map with ID-Blau, the simplified "w/ ID-Blau†" without the diffusion process can still offer an additional gain of 0.47dB over that with "w/ BGAN." This verifies the effectiveness of ID-Blau compared to the GAN-based reblurring model BGAN.

5. Conclusion

We proposed a diffusion-based reblurring model that can take a sharp image and a controllable pixel-wise blur condition map to synthesize a blurred image. To train the reblurring model, we parameterized the blur patterns of a blurred image with their orientations and magnitudes and implicitly represented them in a continuous blur condition field. With the model, we presented ID-Blau, an effective data augmentation scheme for image deblurring, where we sample various blur conditions from the field to produce diverse, realistic blurred images and enrich the training set. Experimental results have shown that ID-Blau can significantly improve the performance of state-of-the-art deblurring models.

6. Acknowledgments

References

[1] Titas Anciukevičius, Zexiang Xu, Matthew Fisher, Paul Henderson, Hakan Bilen, Niloy J. Mitra, and Paul Guerrero. Renderdiffusion: Image diffusion for 3d reconstruction, inpainting and generation. In *CVPR*, 2023. 3

[2] Martin Arjovsky, Soumith Chintala, and Léon Bottou. Wasserstein generative adversarial networks. In *ICML*, 2017. 2

[3] Hanting Chen, Yunhe Wang, Tianyu Guo, Chang Xu, Yiping Deng, Zhenhua Liu, Siwei Ma, Chunjing Xu, Chao Xu, and Wen Gao. Pre-trained image processing transformer. In *CVPR*, 2021. 1

[4] Zheng Chen, Yulun Zhang, Liu Ding, Xia Bin, Jinjin Gu, Linghe Kong, and Xin Yuan. Hierarchical integration diffusion model for realistic image deblurring. In *NeurIPS*, 2023. 3

[5] Zhixiang Chi, Yang Wang, Yuanhao Yu, and Jin Tang. Test-time fast adaptation for dynamic scene deblurring via meta-auxiliary learning. In *CVPR*, 2021. 2

[6] Sung-Jin Cho, Seo-Won Ji, Jun-Pyo Hong, Seung-Won Jung, and Sung-Jea Ko. Rethinking coarse-to-fine approach in single image deblurring. In *ICCV*, 2021. 2, 6

[7] Alexey Dosovitskiy, Lucas Beyer, Alexander Kolesnikov, Dirk Weissenborn, Xiaohua Zhai, Thomas Unterthiner, Mostafa Dehghani, Matthias Minderer, Georg Heigold, Sylvain Gelly, Jakob Uszkoreit, and Neil Houlsby. An image is worth 16x16 words: Transformers for image recognition at scale. In *ICLR*, 2021. 2

[8] Hongyun Gao, Xin Tao, Xiaoyong Shen, and Jiaya Jia. Dynamic scene deblurring with parameter selective sharing and nested skip connections. In *CVPR*, 2019. 1

[9] Sicheng Gao, Xuhui Liu, Bohan Zeng, Sheng Xu, Yanjing Li, Xiaoyan Luo, Jianzhuang Liu, Xiantong Zhen, and Baochang Zhang. Implicit diffusion models for continuous super-resolution. In *CVPR*, 2023. 3

[10] Ian Goodfellow, Jean Pouget-Abadie, Mehdi Mirza, Bing Xu, David Warde-Farley, Sherjil Ozair, Aaron Courville, and Yoshua Bengio. Generative adversarial nets. In *NeurIPS*, 2014. 2

[11] Ishaan Gulrajani, Faruk Ahmed, Martin Arjovsky, Vincent Dumoulin, and Aaron C Courville. Improved training of wasserstein gans. In *NeurIPS*, 2017. 2

[12] Jonathan Ho, Ajay Jain, and Pieter Abbeel. Denoising diffusion probabilistic models. In *NeurIPS*, 2020. 2, 3, 4, 8

[13] Lingshun Kong, Jiangxin Dong, Jianjun Ge, Mingqiang Li, and Jinshan Pan. Efficient frequency domain-based transformers for high-quality image deblurring. In *CVPR*, 2023. 1, 2, 6

[14] Marek Kowalski, Stephan J. Garbin, Virginia Estellers, Tadas Baltrušaitis, Matthew Johnson, and Jamie Shotton. Config: Controllable neural face image generation. In *ECCV*, 2020. 2

[15] Po-Sheng Liu, Fu-Jen Tsai, Yan-Tsung Peng, Chung-Chi Tsai, Chia-Wen Lin, and Yen-Yu Lin. Meta transferring for deblurring. In *BMVC*, 2022. 2

[16] Andreas Lugmayr, Martin Danelljan, Andres Romero, Fisher Yu, Radu Timofte, and Luc Van Gool. Repaint: Inpainting using denoising diffusion probabilistic models. In *CVPR*, 2022. 3

[17] Xudong Mao, Qing Li, Haoran Xie, Raymond Y.K. Lau, Zhen Wang, and Stephen Paul Smolley. Least squares generative adversarial networks. In *ICCV*, 2017. 2

[18] Seungjun Nah, Tae Hyun Kim, and Kyoung Mu Lee. Deep multi-scale convolutional neural network for dynamic scene deblurring. In *CVPR*, 2017. 1, 2, 3, 5

[19] Seungjun Nah, Sanghyun Son, Jaerin Lee, and Kyoung Mu Lee. Clean images are hard to reblur: Exploiting the ill-posed inverse task for dynamic scene deblurring. In *ICLR*, 2022. 2

[20] D. Park, D. U. Kang, J. Kim, and S. Y. Chun. Multi-temporal recurrent neural networks for progressive non-uniform single image deblurring with incremental temporal training. In *ECCV*, 2020. 1

[21] Mengwei Ren, Mauricio Delbracio, Hossein Talebi, Guido Gerig, and Peyman Milanfar. Multiscale structure guided diffusion for image deblurring. In *ICCV*, 2023. 3

[22] Jaesung Rim, Haeyun Lee, Jucheol Won, and Sunghyun Cho. Real-world blur dataset for learning and benchmarking deblurring algorithms. In *ECCV*, 2020. 6

[23] Robin Rombach, Andreas Blattmann, Dominik Lorenz, Patrick Esser, and Björn Ommer. High-resolution image synthesis with latent diffusion models. In *CVPR*, 2022. 3

[24] Chitwan Saharia, Jonathan Ho, William Chan, Tim Salimans, David J. Fleet, and Mohammad Norouzi. Image super-resolution via iterative refinement. *IEEE TPAMI*, 2023. 3

[25] Alon Shoshan, Nadav Bhonker, Igor Kviatkovsky, and Gérard Medioni. Gan-control: Explicitly controllable gans. In *ICCV*, 2021. 2

[26] Jiaming Song, Chenlin Meng, and Stefano Ermon. Denoising diffusion implicit models. In *ICLR*, 2021. 3, 4

[27] Shuochen Su, Mauricio Delbracio, Jue Wang, Guillermo Sapiro, Wolfgang Heidrich, and Oliver Wang. Deep video deblurring for hand-held cameras. In *CVPR*, 2017. 6

[28] Xin Tao, Hongyun Gao, Xiaoyong Shen, Jue Wang, and Jiaya Jia. Scale-recurrent network for deep image deblurring. In *CVPR*, 2018. 1, 2

[29] Zachary Teed and Jia Deng. Raft: Recurrent all-pairs field transforms for optical flow. In *ECCV*, 2020. 3

[30] Hoang Thanh-Tung, Truyen Tran, and Svetha Venkatesh. Improving generalization and stability of generative adversarial networks. In *ICLR*, 2019. 2

[31] Fu-Jen Tsai, Yan-Tsung Peng, Yen-Yu Lin, Chung-Chi Tsai, and Chia-Wen Lin. Stripformer: Strip transformer for fast image deblurring. In *ECCV*, 2022. 1, 2, 6

[32] Ashish Vaswani, Noam Shazeer, Niki Parmar, Jakob Uszkoreit, Llion Jones, Aidan N Gomez, Łukasz Kaiser, and Illia Polosukhin. Attention is all you need. In *NeurIPS*, 2017. 1

[33] Zhendong Wang, Xiaodong Cun, Jianmin Bao, Wengang Zhou, Jianzhuang Liu, and Houqiang Li. Uformer: A general u-shaped transformer for image restoration. In *CVPR*, 2022. 1

[34] Jay Whang, Mauricio Delbracio, Hossein Talebi, Chitwan Saharia, Alexandros G. Dimakis, and Peyman Milanfar. Deblurring via stochastic refinement. In *CVPR*, 2022. 3

[35] Zhisheng Xiao, Karsten Kreis, and Arash Vahdat. Tackling the generative learning trilemma with denoising diffusion GANs. In *ICLR*, 2022. 2

[36] Shaoan Xie, Zhifei Zhang, Zhe Lin, Tobias Hinz, and Kun Zhang. Smartbrush: Text and shape guided object inpainting with diffusion model. In *CVPR*, 2023. 3

[37] Ning Yu, Ke Li, Peng Zhou, Jitendra Malik, Larry Davis, and Mario Fritz. Inclusive gan: Improving data and minority coverage in generative models. In *ECCV*, 2020. 2

[38] Zongsheng Yue, Jianyi Wang, and Chen Change Loy. Resshift: Efficient diffusion model for image super-resolution by residual shifting. In *NeurIPS*, 2023. 3

[39] Syed Waqas Zamir, Aditya Arora, Salman Khan, Munawar Hayat, Fahad Shahbaz Khan, Ming-Hsuan Yang, and Ling Shao. Multi-stage progressive image restoration. In *CVPR*, 2021. 1, 2

[40] Syed Waqas Zamir, Aditya Arora, Salman Khan, Munawar Hayat, Fahad Shahbaz Khan, and Ming-Hsuan Yang. Restormer: Efficient transformer for high-resolution image restoration. In *CVPR*, 2022. 1, 2, 6

[41] Hongguang Zhang, Yuchao Dai, Hongdong Li, and Piotr Koniusz. Deep stacked hierarchical multi-patch network for image deblurring. In *CVPR*, 2019. 1, 2

[42] Kaihao Zhang, Wenhan Luo, Yiran Zhong, Lin Ma, Bjorn Stenger, Wei Liu, and Hongdong Li. Deblurring by realistic blurring. In *CVPR*, 2020. 2, 6, 8